ELSEVIER

Earth and Planetary Science Letters 206 (2003) 21–42

EPSL

www.elsevier.com/locate/epsl

Spatial and temporal distribution of secondary cosmic-ray nucleon intensities and applications to in situ cosmogenic dating

Darin Desilets *, Marek Zreda

Department of Hydrology and Water Resources, University of Arizona, Tucson, AZ 85721, USA

Received 5 July 2002; received in revised form 25 October 2002; accepted 18 November 2002

Abstract

Cosmogenic nuclide production rates depend critically on the spatio-temporal distribution of cosmic-ray nucleon fluxes. Since the 1950s, measurements of the altitude, latitude and solar modulation dependencies of secondary cosmic-ray fluxes have been obtained by numerous investigators. However, until recently there has been no attempt to thoroughly evaluate the large body of modern cosmic-ray literature, to explain systematic discrepancies between measurements or to put these data into a rigorous theoretical framework appropriate for cosmogenic dating. The most important parameter to be constrained is the dependence of neutron intensity on atmospheric depth. Our analysis shows that effective nucleon attenuation lengths measured with neutron monitors over altitudes 0–5000 m range from 128 to 142 g cm^{-2} at effective vertical cutoff rigidities of 0.5 and 14.9 GV, respectively. Effective attenuation lengths derived from thermal neutron data are somewhat higher, ranging from 134 to 155 g cm^{-2} at the same cutoff rigidities and over the same altitudes. We attribute the difference to a combination of two factors: the neutron monitor is more sensitive to the higher end of the nucleon energy spectrum, and the shape of the nucleon energy spectrum shifts towards lower energies with increasing atmospheric depth. We have derived separate scaling models for thermal neutron reactions and spallation reactions based on a comprehensive analysis of cosmic-ray survey data. By assuming that cosmic-ray intensity depends only on atmospheric depth and effective vertical cutoff rigidity, these models can be used to correct production rates for temporal changes in geomagnetic intensity using paleomagnetic records.

Keywords: cosmogenic; scaling; cosmic rays; production rates; neutron monitor

1. Introduction

The reliability of cosmogenic methods of surface exposure dating is limited by the accuracy of nuclide production rates. Ideally, production rates are calibrated on landforms that have simple exposure histories and that have been dated accurately and precisely by independent methods. However, because such landforms are rare, the spatial and temporal coverage of calibrated production rates is limited. Production rates corre-

* Corresponding author. Tel.: +1-520-621-4072; Fax: +1-520-621-1422.
E-mail address: ddesilet@hwr.arizona.edu (D. Desilets).

0012-821X/02/$ – see front matter
PII: S0012-821X(02)01088-9

sponding to a few locations and exposure periods are therefore applied to landforms where the time-averaged cosmic-ray intensity may be different by an order of magnitude or more from the intensity at the calibration site. Differences in cosmic-ray intensity at a sample site and a calibration site are accounted for by multiplying the calibrated production rate by a scaling factor.

Cosmic-ray intensity on Earth varies spatially due to the interaction of primary cosmic rays with terrestrial and interplanetary magnetic fields and because cosmic rays are attenuated by terrestrial matter. Temporal variations are related mostly to changes in geomagnetic, heliospheric and galactic properties that occur on time scales ranging from minutes (e.g. isolated solar flare events) to millennia (e.g. the Earth's magnetic dipole moment). Spatial and temporal variations are linked, since time-dependent variations of the cosmic-ray flux affect some locations on Earth more than others. The 11-yr solar cycle, for example, affects only the cosmic-ray flux at high and mid-latitudes, whereas variations of the geomagnetic dipole intensity affect mainly the mid- and low-latitude flux.

Here, we use measured cosmic-ray fluxes to derive scaling formulas for nucleon-induced spallation reactions and thermal neutron absorption reactions. Our recognition that high-energy neutron reactions and thermal neutron reactions may require different scaling models is an important advance over previous work. Although the models derived by Lal [1], and reported in [2] also imply that scaling models should include the energy dependence of nuclide production (excitation function), Lal [2] gives a parameterization only for the fluxes of nucleons of $E > 40$ MeV. Discrepancies between cosmic-ray surveys conducted with neutron monitors and with unshielded proportional counters (Section 4) suggest that the altitude dependence of cosmogenic nuclide production is more sensitive to energy than was appreciated by Lal [1,2].

The emphasis of this work is on scaling high-energy spallation reactions and thermal neutron absorption reactions. Because the primary data on high-energy nucleons come from neutron monitors, which are also somewhat sensitive to muon fluxes, we derive scaling formulas for fast muon and slow negative muon fluxes so that corrections can be applied to neutron monitor counting rates. These functions can also be used to scale cosmogenic nuclide production by fast and slow muons.

Two important differences between our work (as well as that of [3]) and other models are that we express secondary cosmic-ray fluxes as a function of mass shielding depth (x) in units of g cm^{-2}, in contrast to [2], who used elevation, and as a function of effective vertical cutoff rigidity (R_C) in units of GV, in contrast to [2], who used geomagnetic latitude, and [4] who used geomagnetic inclination. Because x and R_C change over time, the long-term behavior of these parameters must be estimated at both the sample site and the calibration site. The problem of determining R_C from geographic position and magnetic field intensity is discussed later in this paper, whereas the dependence of mass shielding depth on elevation has been discussed by [5,6].

2. Review of scaling models derived from cosmic-ray data

Lal's [1,2] is the most widely cited scaling model. Drawbacks to his pioneering work are that: (1) Cosmic-ray measurements from latitude surveys are ordered according to geomagnetic latitude calculated from an axially symmetric centered dipole model. Such a model does not accurately describe the geomagnetic field's ability to deflect primary cosmic rays [3,4,6]. (2) Atmospheric depth (pressure) data from altitude surveys were converted to elevation using the US standard atmosphere, 1976. The model therefore does not account for spatial variations in the atmospheric pressure structure [4–6]. (3) The model assumes that the shape of the nucleon energy spectrum is independent of altitude at energies below 400 MeV. Measurements performed more recently suggest that the energy spectrum may soften significantly towards sea level, even at energies below 400 MeV [6]. (4) Measurements taken since the 1950s, representing the vast majority of cosmic-ray data, are not included [6,7]. (5) The effects of solar activity are not explicitly addressed [7].

Dunai [4] has proposed a major revision to Lal's [1,2] model. Although his work is more recent than [1,2], Dunai's [4] model is also based on a small subset of the cosmic-ray data from the 1950s [6]. In addition, Dunai [4] orders cosmic-ray data according to geomagnetic inclination, which, like geomagnetic latitude, has a non-unique relation with cosmic-ray intensity [8]. He [4] also neglects the effect of solar activity and implicitly assumes that the energy spectrum is independent of altitude (see discussion in [8]). For these reasons, both the accuracy and reported uncertainty (e.g. $\sim$2% in the sea-level latitude curve) of Dunai's [4] scaling model are questionable.

An important difference between the scaling models of [2] and [4] is the dependence of nucleon fluxes on altitude. Dunai's [4] scaling model consistently gives effective attenuation lengths that are about 5% lower than those calculated from Lal's [2] model. The different attenuation lengths result in a $\sim$10% difference between the two models when production rates are scaled between 1033 and 600 g cm^{-2} (0–5000 m). The two authors also give sea-level neutron fluxes that are different by as much as 12%, even though their scaling models utilize the same sea-level neutron monitor survey [9] as a baseline. Given such discrepancies, and considering the inherent problems with these models, there is an obvious need to investigate the scaling problem in more detail.

Only one published scaling model has been derived entirely from neutron monitor data [10]. That model utilized an extensive survey by Carmichael et al. [11–15] to predict the altitude and latitude dependence of soft fail rates in integrated circuits. Another scaling model for cosmogenic nuclide production based primarily on neutron monitor data (including the results of [11–15]) has been proposed by Lifton [3].

3. Scaling model for spallation reactions

3.1. Data selection

Since the invention of the neutron monitor in the early 1950s, a wide range of atmospheric depths, cutoff rigidities and solar conditions have been measured [7]. These surveys have yielded consistent results, although there exist minor discrepancies due to differences in instrumental responses and experimental procedures.

A good cosmic-ray data set should have the following characteristics: (1) the data should have been collected using similar methods; (2) the experimental methods should be given in detail; (3) the instruments should be well-characterized; (4) the time, date, geographic coordinates and barometric pressure at each measurement location should be recorded; and (5) the data should have extensive coverage in space and time. Corrections for variations in the temperature structure of the atmosphere and high winds (Bernoulli effect) may also improve the quality of a data set [16], but the required meteorological data are often not available for older surveys.

The survey that best meets the criteria above is that conducted by Carmichael and collaborators [11–15] over the International Quiet Sun Year (IQSY), 1965–1966. It comprised 110 measurements of nucleon intensity taken at atmospheric depths of 1033–200 g cm^{-2} (0–12 000 m), and at cutoff rigidities of 0.5–13.3 GV. All measurements at altitudes less than 5000 m ($>$550 g cm^{-2}) were collected with a land-based NM-64 and measurements at higher altitudes were obtained using a cross-calibrated monitor designed for airborne measurements. Neutron monitor counts and counting times are given along with the time, date, barometric pressure, latitude, longitude and effective vertical cutoff rigidity for each location. This survey, described in five back-to-back papers [11–15], is unmatched by any other altitude survey in terms of the detailed experimental description.

Another survey aimed at describing comprehensively the neutron monitor attenuation length (Λ_{NM}) was reported by Raubenheimer and Stoker [17]. To prevent ambient thermal neutrons from reaching the counter, this survey employed an NM-64 monitor with a reflector thickness on all sides double the usual 7.5 cm. There are four important differences between [17]'s survey and that of [11–15]. First, because the reflector thickness was doubled on top, the muon and nucleon en-

ergy sensitivities of the monitor in [17] should be slightly different from that of a standard NM-64 monitor. Second, many of the measurements were taken during the 1969 solar maximum. At high and mid-latitudes ($R_C > 5$ GV) attenuation lengths at solar maximum should be higher by ~ 7 g cm^{-2} than those at solar minimum [17]. Additional measurements were obtained by [17] in 1971, when solar activity was lower than in 1969, but still higher than a typical solar minimum. Third, all measurements were performed from an airplane, most at altitudes greater than 1600 m (< 850 g cm^{-2}). Carmichael et al.'s survey extended to both greater and smaller atmospheric depths [14]. Fourth, and most important for this work, the original counting rates and counting times have not been published by [17]. Nonetheless, despite numerous differences in experimental conditions and approaches, the relation obtained by [17], after normalizing to solar minimum, is in good agreement with the one found by [15], with attenuation lengths that are on average 2% lower than Carmichael and Bercovitch's [15].

Bachelet et al. [18] investigated the dependence of Λ_{NM} on R_C and x by evaluating barometric coefficients (the reciprocal of Λ) calculated from 58 stationary IGY and NM-64 monitors. Unfortunately, they do not give original data (counting rates, counting time, atmospheric pressure) for the neutron monitors, as do [11–15]. Nonetheless, attenuation lengths derived by [18] for solar minimum (1964–1965) are in good agreement with Carmichael and Bercovitch's 1965–1966 results (Fig. 1), despite numerous differences in how the attenuation lengths were derived and the slightly different periods covered [15]. Corrected attenuation lengths from [18] are on average only 1.5% higher than those calculated from our regression to data in [15] (Section 3.4).

Although the measurements of [17,18] are extensive, their data are not as amenable to analysis as Carmichael and Bercovitch's because original counting rates and counting durations are not published. Moreover, discrepancies between [15,17,18] are small and are probably related to minor systematic differences rather than random measurement errors. To attempt to account for these small systematic differences would not be worthwhile in view of larger systematic errors (e.g. energy spectrum and solar activity) involved in applying neutron measurements to cosmogenic nuclides [6].

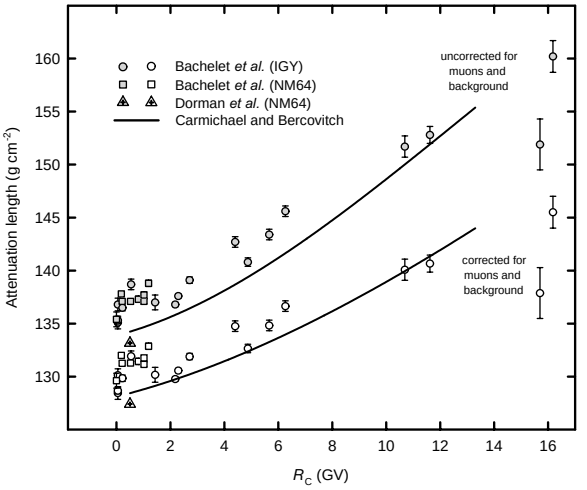

Fig. 1. Attenuation lengths at sea level and solar minimum from neutron monitor attenuation coefficients measured by Bachelet et al. [18], Dorman et al. [20] and Carmichael and Bercovitch [15]. The solid lines are from a surface fitted to Carmichael and Bercovitch's complete data set, which covers a wide range of R_C and x [15].

A precise and rigorous measurement of Λ_{NM} in Antarctica ($R_C < 0.5$) was performed during the 1997 solar minimum survey [16,19,20]. The attenuation length was measured from a ship by recording changes in counting rates caused by small fluctuations in barometric pressure. The neutron monitor counting rate was corrected for the Bernoulli effect, sea-state effect (relevant only to shipborne data) and temperature structure of the atmosphere [19]. The attenuation length derived at this location (Fig. 1) gives us further confidence in the reliability of Carmichael et al.'s data [11–15].

3.2. *Parameterization of attenuation lengths from neutron monitors*

Throughout most of the atmosphere, the altitude dependencies of secondary cosmic-ray fluxes (J) are described by:

$$-\frac{dJ}{dx} = \frac{J}{\Lambda} = \beta J \quad (1)$$

where x is atmospheric depth given in mass-shielding units [g cm^{-2}]. The rate of cosmic-ray absorption is usually expressed by the atmospheric attenuation length, Λ [g cm^{-2}], or its reciprocal, β [cm^2 g^{-1}], the attenuation coefficient. The solution to Eq. 1 is the exponential relation:

$$J_2 = J_1 \exp\left(\frac{x_1 - x_2}{\Lambda}\right) = J_1 \exp(\beta(x_1 - x_2)) \quad (2)$$

where J_1 and J_2 are the fluxes at depths x_1 and x_2. It is sometimes more convenient to use β, which represents the slope of dJ/dx versus J. Because β is a slope, the linear average of all β values over a range of depths x_1 to x_2 gives the effective attenuation coefficient between x_1 and x_2. On the other hand, Λ is often used because it carries the physical significance of being equivalent to the value of Δx over which cosmic-ray flux changes by a factor of e.

Originally, Carmichael and Bercovitch [15] derived the neutron monitor attenuation coefficient, β_{NM}, as a function of R_C and x from the neutron monitor counting rates reported in [11,13]. These results were given graphically, with the relation $\beta_{NM}(R_C,x)$ drawn by hand. Carmichael and Peterson [21] later parameterized Carmichael and Bercovitch's results using polynomials, but they did not report the polynomial coefficients. To make Carmichael and Bercovitch's results useful for scaling spallation reactions, we have parameterized these results in terms of Λ_{NM} using a polynomial [15].

We derived attenuation lengths by following the iterative procedure described by [15] for deriving $\beta_{NM}(R_C,x)$. A sea-level latitude curve was first established from the counting rates at each survey location. Although several survey locations were nominally at sea level, most were at slightly higher elevations and therefore the counting rates had to be reduced (normalized) to sea level. We accomplished this by making an initial estimate for each location of the effective attenuation length (Λ_e) required to reduce the counting rate at x to the sea-level counting rate at the same cutoff rigidity. Then we parameterized the sea-level counting rate, J_{NM}, using the Dorman function [20]:

$$J_{NM}(R_C) = J_0[1 - \exp(-\alpha R_C^{-k})] \quad (3)$$

where J_0 is the high-latitude counting rate, and α and k are fitting parameters. The first approximation to the sea-level latitude curve was then used to calculate $\Lambda_{e,NM}$ for each of the survey locations. A polynomial was fitted to $\Lambda_{e,NM}(R_C,x)$ by the inverse-variance method, and a second approximation to the latitude curve was established. Variances of counting rates were determined by assuming a Poissonian distribution of counting events and using a correction for the multiplicity effect [22]. The procedure was iterated four times, giving a final R^2 of 0.986 (Fig. 2).

The true attenuation length was derived as a continuous function of x from the effective attenuation length by using the relation [15]:

$$\beta(x) = \beta_e(x) + (x - x_0)\frac{\partial \beta_e}{\partial x} \quad (4)$$

where $\beta = 1/\Lambda$, and x_0 is the pressure at sea level.

3.3. Corrections to $\Lambda_{e,NM}$ for muon and background contributions

The contributions of muons and background to the neutron monitor counting rate were removed using the equation:

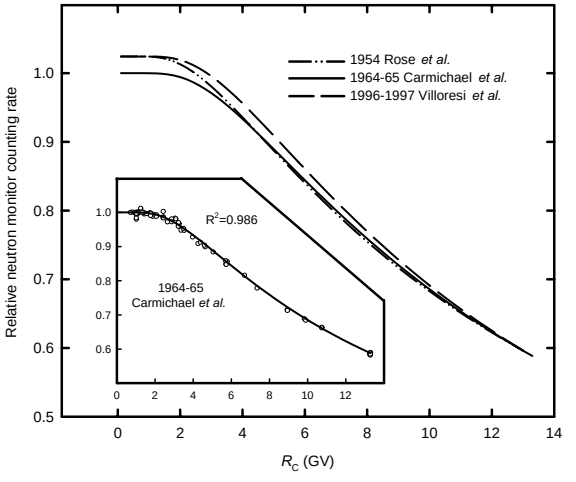

Fig. 2. The sea-level latitude effect at solar minimum, according to Rose et al. [9], Carmichael et al. [11–14] and Villoresi et al. [16], normalized at 13 GV.

Table 1
Relative contributions to the neutron monitor counting rate at high latitude and sea level [57]

	IGY monitor contribution (%)	NM-64 monitor contribution (%)
Neutrons	83.6 ± 2.0	85.2 ± 2.0
Protons	7.4 ± 1.0	7.2 ± 1.0
Pions	1.2 ± 0.3	1.0 ± 0.3
Fast muons	4.4 ± 0.8	3.6 ± 0.8
Slow negative muons	2.4 ± 0.4	2.0 ± 0.4
Background	1.0 ± 0.1	1.0 ± 0.1

$$\frac{1}{\Lambda_{NM}} = \frac{\sum_{i=1}^{n} \frac{C_i}{\Lambda_i}}{\sum_{i=1}^{n} C_i} = \frac{\frac{C_N}{\Lambda_N} + \frac{C_{\mu^-(s)}}{\Lambda_{\mu^-(s)}} + \frac{C_{\mu(f)}}{\Lambda_{\mu(f)}}}{C_N + C_{\mu^-(s)} + C_{\mu(f)} + C_B} \quad (5)$$

where J_i and Λ_i are the counting rate and attenuation length, respectively, for the ith component (note that this equation is incorrect in [6]). At sea level and high latitude, contributions from nucleons (C_N), slow negative muons ($C_{\mu^-(s)}$), fast muons ($C_{\mu(f)}$) and constant background (C_B), account for more than 98% of the neutron monitor counting rate (Table 1).

Fast muon intensity was scaled for altitude and latitude by using a parameterization of fast muon data [7] collected with a muon telescope (MT-64) during the IQSY survey [11,13]. This apparatus consisted of two phosphor scintillators placed above and below an NM-64, with the counting circuits arranged in coincidence. The fast-muon attenuation length, $\Lambda_{\mu(f)}$, is described well ($R^2 = 0.976$) by:

$$\Lambda_{\mu(f)}(R_C, x) = a_0 + a_1 R_C + x(a_2 R_C + a_3) \quad (6)$$

where a_i are fitting coefficients (Table 2). Based on a theoretical range–energy relation [23], muon energies above ~10 GeV are needed to penetrate the 14 cm of lead and 22.5 cm of polyethylene of an NM-64. The sea-level latitude dependence of fast muon intensity (Fig. 3) is much less pronounced than that of the neutron component.

The effective attenuation length for slow negative muons derived by [7] from measurements between 200 and 1033 g cm^{-2} [24–26] is described by:

$$\Lambda_{e,\mu^-(s)}(R_C) = 233 + 3.68 R_C \quad (7)$$

Slow muons are defined here to be those stopping in 117–83 g cm^{-2} of air equivalent, which corresponds to energies below approximately 0.3 GeV [24–26]. Based on [7,27], we assume that the sea-level latitude dependence for slow negative muons is the same as that for fast muons.

3.4. Attenuation lengths for spallation reactions

Based on Carmichael and Bercovitch's neutron monitor data and the corrections described above, the atmospheric attenuation coefficient for high-energy ($E_{med} \sim 120$ MeV) spallation reactions (β_{sp}) is well described by the relation [15]:

$$\beta_{sp}(R_C, x) = \beta_{NM,N}(R_C, x) = n(1 + \exp(-\alpha R_C^{-k}))^{-1} + (b_0 + b_1 R_C + b_2 R_C^2)x + (b_3 + b_4 R_C + b_5 R_C^2)x^2 + (b_6 + b_7 R_C + b_8 R_C^2)x^3 \quad (8)$$

with the coefficients from Table 3. We expressed these results in terms of β rather than Λ for the convenience of calculating effective attenuation lengths. In order to obtain a physically realistic surface (Fig. 4) several parameters in Eq. 8 were constrained during the fitting procedure [7].

The effective attenuation length between two

Table 2
Coefficients for Eq. 6

a_0	2.1658×10^{02}
a_1	8.7830×10^{00}
a_2	-1.3532×10^{-03}
a_3	3.7859×10^{-01}

arbitrary atmospheric depths x_1 and x_2 is calculated from the relation:

$$\Lambda_e(R_C, x_1, x_2) = \frac{\int_{x_1}^{x_2} dx}{\int_{x_1}^{x_2} \beta(R_C, x) dx} \quad (9)$$

and therefore the effective attenuation length for high-energy spallation reactions ($\Lambda_{e,sp}$) between depths x_1 and x_2 is:

$$\Lambda_{e,sp}(R_C, x_1, x_2) = \frac{x_2 - x_1}{\left[\begin{array}{l} n(1+\exp(-\alpha R_C^{-k}))^{-1}\, x + 1/2(b_0 + b_1 R_C + b_2 R_C^2)x^2 \\ + 1/3(b_3 + b_4 R_C + b_5 R_C^2)x^3 + 1/4(b_6 + b_7 R_C + b_8 R_C^2)x^4 \end{array}\right]_{x_1}^{x_2}} \quad (10)$$

Strictly speaking, the parameters in Table 3 are valid only for R_C from 0.5 to 13.3 GV, the limits of Carmichael and Bercovitch's coverage, and x from 1033 to 500 g cm^{-2} [15]. However, our neutron monitor measurements near Bangalore, India in May, 2002 suggest that Eq. 10 can be accurately extrapolated to R_C of 17.25 GV.

3.5. Latitude distribution of spallation reactions at sea level

In order to calculate nucleon fluxes at any point on Earth, the latitude distribution of nucleon fluxes at some reference altitude is needed in addition to Eq. 10. The IQSY sea-level latitude survey (Fig. 2) [11–15] is adequate for this purpose. However, other latitude surveys conducted with neutron monitors (Table 4) provide a check on Carmichael et al.'s sea-level measurements, and extend the available measurements beyond $R_C = 13.3$ GV [11].

Table 3
Coefficients for Eq. 8

n	9.9741×10^{-03}
α	4.5318×10^{-01}
k	-8.1613×10^{-02}
b_0	6.3813×10^{-06}
b_1	-6.2639×10^{-07}
b_2	-5.1187×10^{-09}
b_3	-7.1914×10^{-09}
b_4	1.1291×10^{-09}
b_5	1.7400×10^{-11}
b_6	2.5816×10^{-12}
b_7	-5.8588×10^{-13}
b_8	-1.2168×10^{-14}

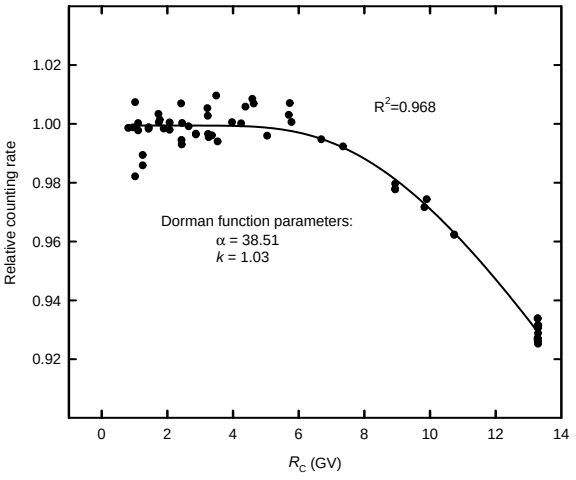

Fig. 3. Dorman function (Eq. 3) fit to sea-level muon monitor counting rates of [11–14].

Because a main motivation for conducting sea-level latitude surveys is the comparison of primary cosmic-ray spectra over different solar minima, most latitude surveys have been conducted during solar quiescence. Their results consistently give a latitude effect (defined here as the ratio of the counting rate at $R_C = 14$ GV to that at $R_C = 0$ GV) of ~ 0.56. Differences between the solar minimum survey reported by [9] (used by both Lal [1,2] and Dunai [4] as a sea-level baseline), the one reported by [11–15], and the most recent one [16] are negligible (Fig. 2) when data are ordered according to R_C, but not when they are ordered according to geomagnetic latitude (λ) [2], geomagnetic inclination (I) [4], or lower cutoff rigidity calculated for a centered dipole field ($R_L^{Störmer}$) [28] (see Section 6).

We suggest using the Dorman function (Eq. 3) parameters obtained from the most recent NM-64 survey [20] (Table 4) to scale spallation reactions, because this survey is the most thorough and because it extends to $R_C = 16.6$ GV.

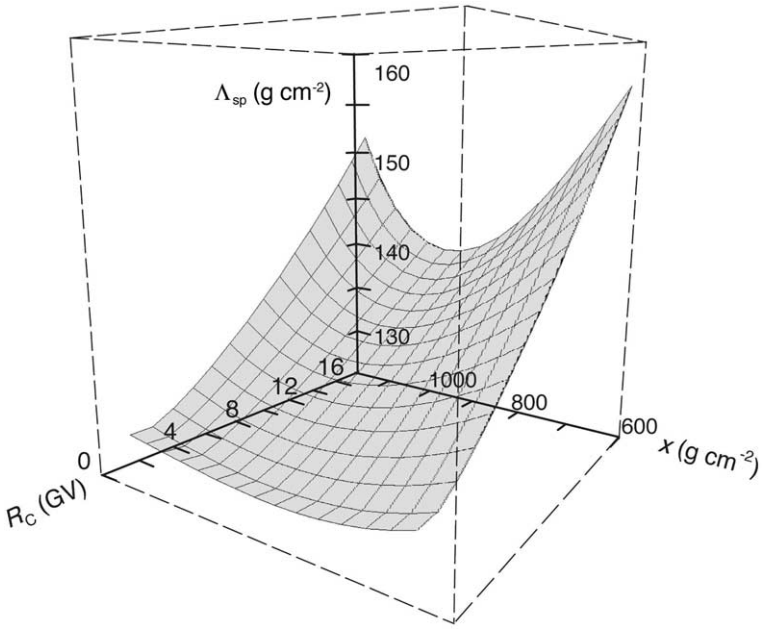

Fig. 4. $\Lambda_{sp}(R_C,x)$ according to Eq. 8. To avoid overfitting the data, this surface was obtained under the constraints: $\partial\Lambda_{sp}/\partial R_C \neq 0$ and $\partial\Lambda_{sp}/\partial x = 0$ only once at any R_c [7].

4. A scaling model for thermal neutron reactions

4.1. Attenuation lengths for thermal neutron reactions

Measurements of neutron multiplicity in neutron monitors and of star-size distributions in cloud chambers and nuclear emulsions suggest that the nucleon attenuation length decreases with increasing energy [6]. However, the importance of this effect at nucleon energies below 400 MeV is uncertain. Data from neutron multiplicity counters suggest that the effect may be important for scaling cosmogenic nuclides [6], contrary to earlier empirical and theoretical evidence [1] and to recent modeling [29]. Although there are currently insufficient data to fully describe the energy dependence of the nucleon attenuation

Table 4
Sea-level latitude surveys of nucleon intensity, 1954–1997

	Year	Type of monitor	α	k	$J_{NM}^{Rc=14\ GV}/J_{NM}^{Rc=0\ GV}$	Source
Solar minimum	1954	IGY	8.241	0.8756	0.56	[9][a]
	1965	IGY	9.236	0.9146	0.56	[58][a]
	1965	NM-64	9.819	0.9288	0.57	[11][a]
	1974	NM-64	7.28	0.83	0.56	[59]
	1976	NM-64	8.953	0.9159	0.55	[60][a]
	1987	NM-64	10.068	0.9519	0.56	[61]
			10.446	0.9644	0.56	
	1997	NM-64	10.275	0.9615	0.56	[20]
		BC[b]	9.694	0.9954	0.50	
Solar maximum	1969	NM-64	7.79	0.83	0.58	[59]
	1981	9-NMD[c]	10.88	0.92	0.62	

[a] Parameters reported by [61].
[b] Unshielded BF_3 proportional counter (sensitive to thermal neutrons).
[c] Leadless neutron monitor.

length, it is likely that differences between attenuation lengths for most spallation reactions should be only 1–2 g cm^{-2}. Because this is smaller than uncertainties of empirical data, a single parameterization can be used to describe attenuation lengths for spallation reactions. However, the difference between attenuation lengths for thermal neutron reactions, Λ_{th}, and those for spallation reactions, Λ_{sp}, may be significant.

Although the altitude dependencies of fast and thermal neutron fluxes have been measured in several studies [30–33], reliable data are limited mostly to high altitudes (<600 g cm^{-2}, >4350 m). Because the fluxes of fast neutrons ($E\sim1$ MeV) and thermal neutrons ($E<0.5$ eV) have been experimentally shown to be in equilibrium [31], in this paper we consider attenuation lengths for fast neutrons (Λ_f) and thermal neutrons (Λ_{th}) to be equivalent. These energies are substantially below the ~40 MeV required to induce spallation reactions [2]. Note that our use of the term 'fast neutron' is different from most of the cosmogenic literature but is consistent with definitions from nuclear physics (see [6] for definitions of fast neutrons and high-energy neutrons).

One of the most extensive surveys of thermal neutrons was a series of balloon flights carrying unshielded proportional counters [31]. Attenuation lengths reported by [31] agree well with airplane and balloon measurements of fast neutrons performed later [32] and with earlier values of Λ_{th} obtained with a shielded thermal neutron detector [30] over the range 200–600 g cm^{-2}. Unfortunately, these surveys were restricted to atmospheric depths less than 715 g cm^{-2} (>3200 m), and the data obtained at depths greater than 400 g cm^{-2} (<5750 m) have large uncertainties.

A comparison of attenuation lengths measured by shielded and unshielded proportional counters with those measured independently by neutron monitors strongly suggests that the fluxes of neutrons of $E>100$ MeV and those of $E<10$ MeV (Table 5) attenuate in the atmosphere at different rates. These results are consistent with an energy spectrum that softens toward sea level. The magnitude of the difference between low- and high-energy nucleon attenuation lengths measured in the upper atmosphere is too large to be attributed to either solar activity or any known instrumental bias other than energy sensitivity [6].

In a more recent airborne survey [33], which extended to lower elevation than previous surveys [30–32], fast neutron fluxes were measured with proportional counters shielded by 7.5 and 12.5

Table 5
Comparison of $\Lambda_{e,th}$ and $\Lambda_{e,f}$ from various surveys with $\Lambda_{e,sp}$ from Eq. 10

	Year	Δx[a] (g cm^{-2})	R_C[b] (GV)	$\Lambda_{e,th/f}$ (g cm^{-2})	$\Lambda_{e,sp}$ (g cm^{-2})
[30]	1947–49	200–600	<0.5	157	132
			1.7	157	132
			3.0	181	134
			11.5	206	151
			13.5	212	155
[31]	1952–54	200–715	<0.5	164	131
			1.4	164	138
			13.7	212	152
[32]	1964–71	200–715	<0.5	163 ± 10	132
			<0.5	172 ± 13	132
			4.5	181 ± 28	141
			17.0	215 ± 28	163
[33,34]	1969	200–715	3.1	149	132
			4.9	155	134
			7.3	163	141
			11.7	182	149
			14.2	195	153

[a] Measurements are not necessarily evenly spaced throughout Δx.
[b] Cutoff rigidities for [30] and [31] were interpolated from grid values for 1955 [62] or taken directly from [49].

cm of paraffin. The relation between Λ_{th} and atmospheric depth was fitted to a linear regression by [33] (also reported in [34]). Throughout most of the atmosphere, Λ_{th} measured by [33] is greater than $\Lambda_{NM,N}$ (Eq. 10), but at high cutoff rigidities, the relationship is reversed near sea level (Fig. 5). This result is difficult to explain, since it would imply that the energy spectrum of the omnidirectional neutron flux hardens with depth in the lowermost 1000 m of atmosphere. This behavior is probably incorrect and can be explained by a lack of data near sea level (Mischke's measurements extend from 307 g cm^{-2} (9500 m) to 960 g cm^{-2} (680 m) [33]). To correct for this probable artifact of Mischke's regression [33], we modified his relationship so that Λ_{th} is always larger than or equal to $\Lambda_{NM,N}$, even at depths greater than $\sim$900 g cm^{-2} ($<$985 m) (Fig. 5). The attenuation coefficient for thermal neutron fluxes in the depth range 500–1033 g cm^{-2} is given by:

$$\beta_{th}(R_C, x) = c_0 + c_1 R_C + c_2 R_C^2 + (c_3 + c_4 R_C)x + (c_5 + c_6 R_C)x^2 + (c_7 + c_8 R_C)x^3 \quad (11)$$

and the parameters c_i are in Table 6. The effective attenuation length over the depth interval x_1 to x_2 is given by:

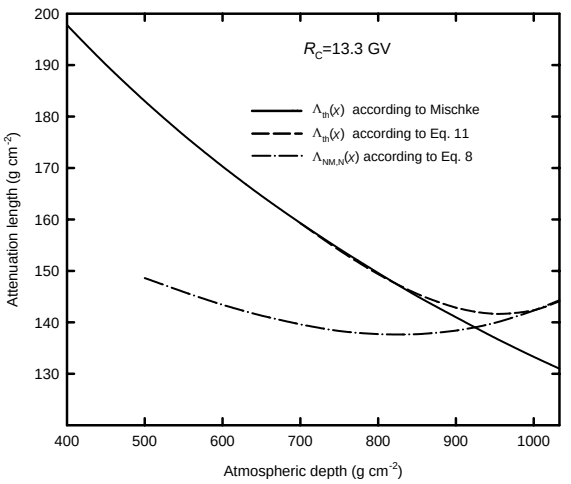

Fig. 5. Thermal neutron attenuation lengths at $R_C = 13.3$ GV [33], with correction at low altitude.

$$\Lambda_{e,th}(R_C, x_1, x_2) = \frac{x_2 - x_1}{\left[(c_0 + c_1 R_C + c_2 R_C^2)x + 1/2(c_3 + c_4 R_C)x^2 + 1/3(c_5 + c_6 R_C)x^3 + 1/4(c_7 + c_8 R_C)x^4 \right]_{x_1}^{x_2}} \quad (12)$$

Simultaneous measurements during a 1996–1997 sea-level latitude survey [20] confirm that Λ_{th} approaches Λ_{NM} toward sea level. Aboard a ship in Antarctica, Λ_{th} was found to be 131 $\pm$ 2 g cm^{-2}, which is indistinguishable from the value of 129 $\pm$ 1 g cm^{-2} for Λ_{NM} (after removing the contribution of muons according to Eq. 5 and Table 1) [20].

Attenuation lengths reported by [33] are about 10% lower than attenuation lengths reported by others [30–32] for the fast and thermal neutron fluxes. The reason for this difference may be that Mischke's instrument was more sensitive to neutrons of higher energy [33]. However, given that Λ_{th} changes rapidly with atmospheric depth and that [30–32] lack data in the lower atmosphere, it is probably more accurate to use Mischke's results than to extrapolate the attenuation lengths of [30–32] to sea level [33].

4.2. *Latitude distribution of thermal neutron reactions at sea level*

The only reliable latitude data for thermal neutron fluxes is the 1996–1997 sea-level latitude survey that carried two bare BF_3 thermal neutron counters along with the usual NM-64 [16]. The 10% greater latitude effect measured with the bare counters implies that sea-level latitude distribution of thermal neutron reactions (e.g. $^{35}Cl(n,\gamma)^{36}Cl$ and $^{40}Ca(n,\gamma)^{41}Ca$) should also be scaled separately from spallation reactions (Table 4). We therefore suggest using the Dorman function (Eq. 3) parameters corresponding to the 1997 bare counter (BC) survey as a baseline for scaling thermal neutron fluxes.

5. Solar activity

Nucleon attenuation lengths measured at high

Table 6
Coefficients for Eq. 11

c_0	5.4196×10^{-03}
c_1	2.2082×10^{-04}
c_2	-5.1952×10^{-07}
c_3	7.2062×10^{-06}
c_4	-1.9702×10^{-06}
c_5	-9.8334×10^{-09}
c_6	3.4201×10^{-09}
c_7	4.9898×10^{-12}
c_8	-1.7192×10^{-12}

latitudes [18,35] exhibit a strong dependence on solar activity. This dependence is related to changes in the energy spectrum of secondary nucleons and to variations in the relative contributions of muons, background and nucleons to the neutron monitor counting rate. As solar modulation increases, the primary energy spectrum hardens, and secondary cascades tend to penetrate more deeply into the atmosphere. Although the total counting rate of a neutron monitor decreases with increasing solar modulation, the proportion of counts from muons increases because muons have a high-energy progenitor that is less sensitive to solar modulation than is the nucleon flux.

The dependence of $\Lambda_{e,NM,N}$ on solar activity was measured by Raubenheimer and Stoker [35] at $R_C = 4.9$ and 8.3 GV. These results, expressed as the percent increase in the neutron monitor attenuation length ($\%\Delta\Lambda_{e,NM,N}$) over the solar minimum value due to an increase in solar activity, are represented by:

$$\%\Delta\Lambda_{e,MN,N}(C_{DR}, R_C) = d_0 + d_1 C_{DR} + d_2 C_{DR}^2 + (d_3 + d_4 C_{DR}) R_C + (d_5 + d_6 C_{DR}) R_C^2 + (d_7 + d_8 C_{DR}) R_C^3 \quad (13)$$

where C_{DR} is the counting rate of the Deep River, Ontario neutron monitor ($R_C = 1.02$ GV, $x = 1016$ g cm^{-2}) relative to that in May 1965; the values of the coefficients are given in Table 7. Raubenheimer and Stoker [35] found that changes in $\Lambda_{e,NM,N}$ over the solar cycle are independent of x, [18] found the dependence to be stronger at greater atmospheric depths, and [21] found the dependence to be greater at smaller atmospheric depths [35]. Raubenheimer and Stoker [35] measured the greatest overall change in attenuation length from solar maximum to solar minimum. Given that experimental results have been contradictory, additional measurements of the time dependence of neutron monitor attenuation lengths are needed.

The usefulness of Eq. 13 for geological applications is limited by the lack of a well-constrained solar modulation record for times older than ~400 yr BP. There is some promise that records of atmospheric radionuclides deposited in sediments and tree rings can shed light on past solar modulation; however, the solar-activity signal in these records is often obscured by natural processes on Earth. Although the behavior of solar modulation in the geologic past is not well known, observations of solar modulation over the past 50 years place reasonable limits on the range of the likely effective (integrated) solar modulation levels for the past several hundreds of thousands of years.

6. Temporal geomagnetic correction

Geomagnetic dipole intensity changes over time [36] and so, therefore, do cutoff rigidities over much of the Earth. The magnitude of the temporal variation in geomagnetic shielding depends on latitude; low latitudes experience stronger fluctuations in primary intensity than do high latitudes. Near the geomagnetic poles, where the magnetic field is mostly in the vertical direction, vertically incident primaries are admitted to the Earth regardless of dipole intensity.

Table 7
Coefficients for Eq. 13

d_0	$4.5414\times10^{+01}$
d_1	$-4.1363\times10^{+01}$
d_2	$-4.1691\times10^{+00}$
d_3	$-4.9907\times10^{+00}$
d_4	$5.0619\times10^{+00}$
d_5	3.3590×10^{-01}
d_6	-3.4601×10^{-01}
d_7	-1.0562×10^{-02}
d_8	1.0964×10^{-02}

Time-averaged R_C (and also λ and I, which serve analogous functions) can be calculated from geomagnetic field models. For durations longer than 20 000 yr, a geocentric axial dipole field is usually assumed (the GAD hypothesis) (e.g. [4,37,38]). The basis of the GAD hypothesis is that higher-order components of the geomagnetic field are short-lived, and that over the long term, transitory non-dipole features have canceling effects, so that the field averages to a simple dipole. Terrestrial and marine records of the intensity and position of this assumed dipole are available from several authors (e.g. [36,39–42]).

In this section we demonstrate how the scaling models derived in Sections 3 and 4 can be used to correct for fluctuations in dipole intensity. We assume that an accurate paleointensity record is available and that for periods greater than 20 000 yr the GAD hypothesis is valid. Although additional work is needed to constrain the paleomagnetic record and to determine the minimum averaging period necessary for the GAD hypothesis to apply, these issues will not be discussed here. Also, we disregard the effects of solar modulation, as did previous investigators working with empirical data [2,4].

Several investigators have explicitly addressed the problem of correcting cosmogenic nuclide production rates for temporal fluctuations in dipole intensity and position. Bierman and Clapp [43] developed a correction model based on Lal's scaling formula and published field strength/rigidity relationships [2]. Licciardi et al. [37] investigated the effects of polar wander on production rates at 44.3°N latitude. Liciardi et al. [37] and Phillips et al. [44] considered the effects of variations in the dipole intensity and concluded that they are negligible for their mid-latitude locations.

Shanahan and Zreda [38] gave the first published description of a dipole intensity correction at the geomagnetic equator. This correction utilized Lal's scaling model and a relation between global atmospheric production rates of cosmogenic nuclides (Q) and magnetic dipole intensity (M) given by [2,45]:

$$\frac{Q}{Q_0} = \left(\frac{M}{M_0}\right)^{0.52} \tag{14}$$

This expression was derived from a numerical integration over all latitudes of a first-order analytical relation describing primary particle motion in a dipole field.

The geomagnetic correction model described in this section improves on previous approaches [38,43] in two important ways: it is based on a model that better describes the current distribution of cosmic-ray intensity and it does not rely on Eq. 14.

The applicability of Eq. 14 to scaling in situ cosmogenic production rates is limited by several factors. First, in deriving Eq. 14 Elsasser et al. [45] assumed that the nuclide production per primary cosmic-ray particle in a column of atmosphere is independent of primary energy. This allowed [45] to assume that global production is a function only of the total primary cosmic-ray flux. However, later work [46] showed that nuclide production per primary particle increases by a factor of 2.7 from 60° to 0° geomagnetic latitude, and therefore that the energy spectrum of primaries is an important factor in global cosmogenic nuclide production. Second, Elsasser et al. [45] assumed a simple power law function for the integral primary energy spectrum that was based on early data from the 1940s and early 1950s. Better estimates (e.g. [47]) are now available. Unfortunately, these assumptions, which were explicitly stated by [45], are often overlooked. Third, the greatest obstacle to using Eq. 14 is that there is no rigorous way to relate the dipole-intensity dependence of global production rates to local production rates using Lal's [2] scaling model, because the parameterization given by [2] is valid only to an altitude of 10 km ($\sim$260 g cm^{-2}), whereas most atmospheric cosmogenic nuclides are produced at altitudes above 10 km [46].

Recently, Dunai [28] proposed a temporal geomagnetic scaling model based on measurements of paleo-inclination and paleo-horizontal field intensity at a sample site. This model uses a relation derived by Rothwell [48] from the Störmer equation for the lower cutoff rigidity of a primary proton in an axial-dipole field:

$$R_L^{\text{Störmer}}(\lambda_{\text{dpl}}) = \frac{30}{4r_e^2} M_0 \cos^4 \lambda_{\text{dpl}} \text{ [GV]} \tag{15}$$

where $R_L^{Störmer}(\lambda_{dpl})$ is the Störmer lower cutoff rigidity as a function of geomagnetic latitude in a dipole field (λ_{dpl}), r_e [m] is the radius of the Earth and M_0 [A m^2] is the dipole intensity. Rothwell [48] substituted λ_{dpl} in Eq. 15 with geomagnetic inclination (I_{dpl}) using a relation that applies only to a dipole field:

$$\tan I_{dpl} = 2\tan \lambda_{dpl} \quad (16)$$

He also substituted a relation between dipole intensity and horizontal field intensity (H_{dpl}) that is valid only for a dipole field:

$$H_{dpl} = M_0 r_e^{-3} \cos \lambda_{dpl} \quad (17)$$

The result is a relation between $R_L^{Störmer}$, horizontal field strength and magnetic inclination:

$$R_L^{Störmer}(I_{dpl}, H_{dpl}) = \frac{30}{4} r_e^2 \frac{H_{dpl}}{1 + \frac{1}{4}\tan^2 I_{dpl}} \text{ [GV]} \quad (18)$$

Because the geomagnetic field far from the Earth influences primary cosmic-ray trajectories, it is always necessary to assume a model of the entire geomagnetic field when calculating cutoff rigidity. In applying Eq. 18 to the real geomagnetic field, one assumes that R_L can be estimated by replacing the Earth's complex (short-term) magnetic field with a dipole whose magnitude and direction are determined only by the magnitude and direction of the local surface field [48]. Rothwell [48] recognized that the path of a cosmic-ray particle is determined not only by the field at the surface, but also by the main dipole field, and suggested that the value of R_C should lie between $R_L^{Störmer}(\lambda_{dpl})$ and $R_L^{Störmer}(I,H)$, where I and H are calculated from the real magnetic field. Due to the inherent limitations of Eq. 18, Rothwell [48] advocated using this expression *only* in conjunction with an empirical relation that he gives in [48]. He showed that Eq. 18 does not satisfactorily align cosmic-ray data from different latitude transects into a unique relationship (Fig. 6). The inadequacy of $R_L^{Störmer}(I,H)$ is also demonstrated by Dunai's figure 1 in [4], which shows a non-unique relation between cutoff rigidity and nucleon intensity (cosmic-ray intensity varies by 12% between some locations at constant $R_L^{Störmer}$ (I,H)) and Dunai's figure 1 in [28], which suggests that at 620 g cm^{-2} (4300 m) nucleon intensity is nearly constant with increasing cutoff rigidity beyond 12 GV. The physical reality is that the Earth's magnetic field at large distances (many Earth radii) influences cosmic rays, and that knowledge of the surface field is useful only insofar as it helps to constrain models of the entire geomagnetic field. Because Eq. 18 poorly accounts for the distribution of cosmic rays in the present geomagnetic field (Fig. 6), it should be used with caution in paleomagnetic fields, and its limitations should be well understood.

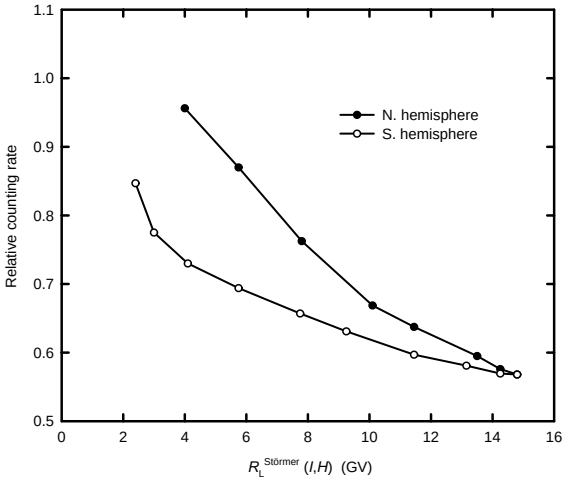

Fig. 6. Neutron monitor counting rates at sea level ordered according to $R_L^{Stormer}(I,H)$ where I and H are from the surface field [48].

6.1. Geomagnetic scaling based on R_C

The problem of scaling production rates for fluctuations in dipole intensity is simplified when cosmic-ray data are ordered according to R_C. R_C is calculated by tracing cosmic-ray trajectories in a model of the geomagnetic field [49]. If we assume that cosmic-ray intensity at a given atmospheric depth is a unique function of R_C, then the main challenge is calculating R_C for past epochs at the sample site and calibration site. This assumption allows recent cosmic-ray measurements to be directly applied to paleomagnetic fields.

Usually the approximation is made that over

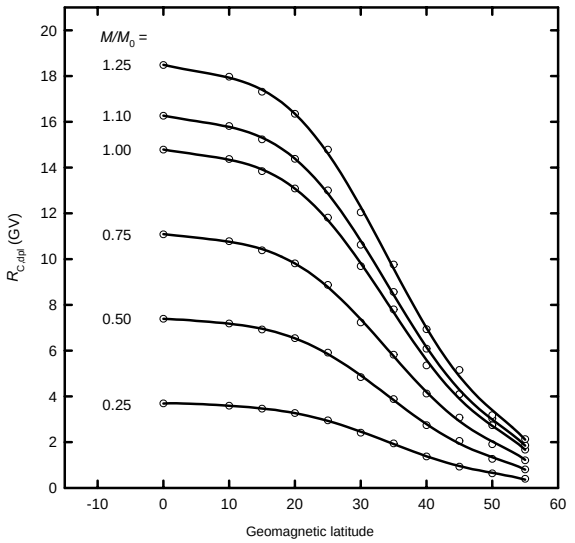

Fig. 7. The latitude dependence of R_C in an axially symmetric centered-dipole field at dipole intensities ranging from 0.25 to 1.25 times the 1945 reference value ($M_0 = 8.084 \times 10^{22}$ A m^2 [50]). The lines are according to Eq. 19.

periods greater than ~20 000 yr, the average behavior of the geomagnetic field converges to an axially symmetric centered-dipole field [4,29,37] with an integrated dipole intensity that depends on the exposure period. We therefore calculated R_C for an axially symmetric centered-dipole field having an intensity ranging from 1.25 to 0.25 times the 1945 value of 8.084×10^{22} A m^2 [50] (Fig. 7). We used the numerical trajectory tracing code and the methods described by [20,49] to trace the paths of anti-protons analytically ejected from the Earth in the vertical direction. Particles escaping the geomagnetic field to infinity correspond to the trajectories of primary cosmic-ray protons that are admitted to the Earth. The lower, upper and effective cutoffs (R_L, R_U and R_C) were calculated by tracing particles at 0.01 GV intervals. R_C was calculated by subtracting the total of the allowed rigidity intervals from the highest forbidden rigidity interval (R_U) (Fig. 8). These results are described ($R^2 > 0.999$) by:

$$R_{C,dpl} = \sum_{i=1}^{i=6} \left(e_i + f_i \left(\frac{M}{M_0} \right) \right) \lambda_{dpl}^{(i)} \qquad (19)$$

with the parameters from Table 8. These parameters are valid between $\lambda_{dpl} = 0°$ and 55°. Above $\lambda_{dpl} = 55°$, cosmic-ray fluxes are unaffected by changes in dipole intensity. Note that in Eq. 19, λ_{dpl} is raised to the ith power.

For the special case in which the GAD hypothesis is invalid and a time series of I and H is available at the sample site, but data at other locations are too few to constrain the entire field, there are several methods of calculating either the lower vertical cutoff rigidity or effective vertical cutoff rigidity. Based broadly on the methods proposed by [48] and partially adopted by [28], we calculated cutoff rigidities using three approaches. The first approach assumes an axially symmetric centered-dipole field with a known pole position. The second approach assumes a centered-dipole field with the axial position determined only by a local value of I and H. The third approach is to take the mean of the values from the first two approaches. For each of these approaches, we separately applied Eqs. 15 and 19.

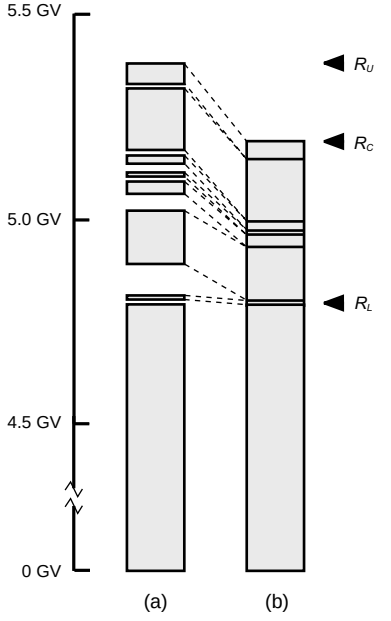

Fig. 8. (a) The penumbral structure for vertically incident cosmic-ray protons, 20 km above Tucson, AZ (32.1°N, 249.1°E) calculated by tracing cosmic-ray trajectories through International Geomagnetic Reference Field 1995. Forbidden rigidity intervals are shaded. (b) R_C is calculated by subtracting the sum of the allowed rigidity intervals from R_U.

Table 8
Coefficients for Eq. 19

	e_i	f_i
$i=0$	-4.3077×10^{-03}	$1.4792\times10^{+01}$
1	2.4352×10^{-02}	-6.6799×10^{-02}
2	-4.6757×10^{-03}	3.5714×10^{-03}
3	3.3287×10^{-04}	2.8005×10^{-05}
4	-1.0993×10^{-05}	-2.3902×10^{-05}
5	1.7037×10^{-07}	6.6179×10^{-07}
6	-1.0043×10^{-09}	-5.0283×10^{-09}

Cutoff rigidities were calculated on a 5° latitude by 15° longitude grid using a 10th degree spherical harmonics representation of International Geomagnetic Reference Field (IGRF) 1980. We compared these results to effective vertical cutoff rigidities calculated by [51] for IGRF 1980. The purpose of the calculations was to determine which method gives the closest approximations of cutoff rigidities derived by trajectory tracing, and to quantify the discrepancies (Table 9). Effective vertical cutoffs calculated from an average of the first and second methods proved superior, with the estimated vertical cutoff rigidity being on average within 1 GV and no more than 3.5 GV from the true value [51]. Cutoffs calculated using Eq. 15 for lower cutoff rigidity also give a reasonable, but slightly less accurate approximation to R_C. The uncertainty in applying each of these methods to real cosmogenic dating scenarios is difficult to assess, since the position of the magnetic poles and local measurements of I and H have associated uncertainties (which may be correlated), and since errors in paleo-cutoff rigidity estimates tend to have canceling effects over large integration periods.

6.2. Calculating time-integrated cosmic-ray fluxes

The equations ordinarily used for interpreting cosmogenic radionuclide data assume that the production rate (P) at a sample location is constant with time [2,52]. This approximation allows for a straightforward analytical solution to the problem of calculating exposure age (t) from measured sample inventories of spallogenic nuclides (N_{meas}) [2,52]:

$$N_{meas} = \left(\frac{P_{sp}}{\lambda_{dec}+\varepsilon/\Lambda_{sp,ss}}\right)\exp(-x_{ss}/\Lambda_{sp,ss})\,[\exp(\varepsilon t/\Lambda_{sp,ss})-\exp(-t(\lambda_{dec}+\varepsilon/\Lambda_{sp,ss}))]+N_0\exp(-\lambda_{dec}t) \quad (20)$$

where P_{sp} is the production rate of a spallogenic nuclide at the land surface, ε is the erosion rate [g cm^{-2} yr^{-1}], λ_{dec} is the decay constant, x_{ss} is the depth of a sample below the Earth's surface [g cm^{-2}], $\Lambda_{sp,ss}$ is the effective subsurface attenuation length for spallogenic nuclide production [g cm^{-2}] and N_0 is the inherited inventory.

The time dependence of production rates can be taken into account by discretizing the exposure period into n time intervals of width Δt_i, and calculating an effective production rate ($P_{sp}^{\Delta t_i}$) over each Δt_i. The equation relating exposure age to production rates [2] is then given by:

$$N_{calc} = \sum_{i=1}^{i=n}\left(\frac{P_{sp}^{\Delta t_i}}{\lambda_{dec}+\varepsilon/\Lambda_{sp,ss}}\right)\exp(-x_{ss}/\Lambda_{sp,ss})\,[\exp(\varepsilon\Delta t_i/\Lambda_{sp,ss})-\exp(-\Delta t_i(\lambda_{dec}+\varepsilon/\Lambda_{sp,ss}))]+N_{\Delta t_{i-1}}\exp(-\lambda_{dec}\Delta t_i) \quad (21)$$

where $N\Delta t_{i-1}$ is the inventory from the preceding time step. For $i=1$, $N\Delta t_{i-1}$ corresponds to the inherited inventory.

Eqs. 20 and 21 require additional terms if thermal and epithermal neutron reactions are important, as in the production of ^{36}Cl [52]. The depth dependencies of thermal and epithermal neutron fluxes follow the form of a triple exponential: $A\exp(-Bx)+C\exp(-Dx)+E\exp(-x/\Lambda_{th,ss})$, where the parameters A, B, C, D and E for a given material are calculated from physical and chemical properties [53], and $\Lambda_{th,ss}$ is the subsurface attenuation length for thermal neutron reactions, which can be assumed to be the same as for spallation reactions. If the profile of combined epithermal and thermal neutron production can be fitted to a single triple-exponential function, then the discretized form of the buildup equation for

Table 9
A comparison of methods of estimating R_C from limited geomagnetic data

	Field model/method	Average residual (GV)	Average absolute residual (GV)	Maximum absolute residual (GV)
$R_L^{Störmer}$	(a) axially Storsymmetric centered dipole	0.6	2.0	6.9
	(b) centered dipole with pole at 78.81°N	0.6	2.5	5.4
	(c) dipole field constructed from surface values of I and H	0.4	1.5	5.7
	(d) average R from (b) and (c)	0.5	1.0	4.5
$R_{C,dpl}$	(a) axially symmetric centered dipole	0.0	1.9	5.3
	(b) centered dipole with pole at 78.81° N	0.0	1.4	4.9
	(c) dipole field constructed from surface values of I and H	−0.21	1.4	5.5
	(d) average of (b) and (c)	0.0	0.8	3.5

The average residual is the average difference between R_C calculated by [51] on a 5° latitude by 15° longitude grid for the IGRF 1980 field and R estimated for the same field by the methods listed below. These comparisons cover the range −55° and 55° latitude.

combined thermal, epithermal and spallogenic production is:

$$N_{calc} = \sum_{i=1}^{i=n} \left(\frac{P_{sp}^{\Delta t_i}}{\lambda_{dec} + \varepsilon/\Lambda_{sp,ss}} \right) \exp(-x_{ss}/\Lambda_{sp,ss}) \left[\exp(\varepsilon \Delta t_i/\Lambda_{sp,ss}) - \exp(-\Delta t_i(\lambda_{dec} + \varepsilon/\Lambda_{sp,ss})) \right] + \left(\frac{P_{th}^{\Delta t_i}}{\lambda_{dec} + B\varepsilon} \right) A \exp(-Bx_{ss}) \left[\exp(B\varepsilon \Delta t_i) - \exp(-\lambda_{dec} \Delta t_i) \right] + \left(\frac{P_{th}^{\Delta t_i}}{\lambda_{dec} + D\varepsilon} \right) C \exp(-Dx_{ss}) \left[\exp(D\varepsilon \Delta t_i) - \exp(-\lambda_{dec} \Delta t_i) \right] + \left(\frac{P_{th}^{\Delta t_i}}{\lambda_{dec} + \varepsilon/\Lambda_{th,ss}} \right) E \exp(-x_{ss}/\Lambda_{th,ss}) \left[\exp(\varepsilon \Delta t_i/\Lambda_{th,ss}) - \exp(-\lambda_{dec} \Delta t_i) \right] + N_{\Delta t_{i-1}} \exp(-\lambda_{dec} \Delta t_i) \quad (22)$$

For each additional production mechanism having an exponential depth dependence in the subsurface (e.g. slow negative muons and fast muons), an additional term of the same form as the first terms on the right-hand sides of Eqs. 21 and 22 may be added, with the subsurface attenuation length for that component substituted for Λ_{ss}. The production rates for fast muons and slow muons can be scaled from the calibration site to the sample site using the scaling formulas in Section 3.3.

The exposure duration is found by calculating the number of time steps (n) needed to make the calculated nuclide inventory for a sample, N_{calc}, equal to the measured nuclide inventory of a sample (N_{meas}):

$$t = n\Delta t_i \quad (23)$$

Because the accuracy of Eq. 23 depends on the size of the time steps, it may be necessary to make Δt_i smaller than would be justified by the resolution of the geomagnetic record alone.

A first approximation to the surface exposure age (t_{app}) can be calculated from Eqs. 20–22 by neglecting geomagnetic effects. A second approximation of n is obtained from $t_{app}/\Delta t_i$. This value of n is then used in Eq. 21 or Eq. 22 to calculate a first approximation of N_{calc}. If $N_{calc} > N_{meas}$ then n should be decreased on the next iteration. If $N_{calc} < N_{meas}$ then n should be increased. This iterative procedure yields exposure ages that converge on the true exposure age.

Eqs. 21 and 22 require knowledge of the production rate at a sample site over each time step. A calibrated production rate (P_{clb}) corresponding to a different location and exposure period can be used at any given sample site if differences in atmospheric shielding, cutoff rigidity, topographic shielding, and sample depth are taken into account by applying scaling factors:

$$P^{\Delta t_i} = f_{topo} f_{ss} f_{R_C,x}(\Delta t_i) P_{clb} \quad (24)$$

The factor f_{topo} accounts for differences in topographic shielding and exposure angle at the sam-

ple site and calibration site. If both sample site and calibration site are flat and unobstructed, $f_{topo} = 1$. The factor f_{ss} normalizes the subsurface production rate at the calibration site to surface production rate. Since most of the reported production rates are already normalized to the surface value, f_{ss} is usually equal to 1. The factor $f_{R_C,x}(\Delta t_i)$, which accounts for differences in x and R_C between calibration site and sample site, may have a strong time dependence and therefore should be calculated for each Δt_i. This scaling factor is given by:

$$f_{R_C,x}(\Delta t_i) = \frac{J_{clb}^{avg}}{J(\Delta t_i)} \quad (25)$$

where J_{clb}^{avg} is the average cosmic-ray flux at the calibration site and $J(\Delta t_i)$ is the cosmic-ray flux at the sample site during time interval i. In applying Eq. 25, it is necessary to know only the relative nucleon fluxes, which can be calculated from the effective attenuation lengths and latitude curves in Sections 3 and 4. The average cosmic-ray flux at the calibration site is given by:

$$J_{clb}^{avg} = \frac{\int J_{clb}(R_C, x)\mathrm{d}t}{\int \mathrm{d}t} \quad (26)$$

which must be integrated numerically over the exposure duration of the calibration site. A sample calculation demonstrating our geomagnetic procedure is available as a **Background Data Set**[1].

Temporal variations in dipole intensity can also be accounted for in a less rigorous way by calculating a single effective production rate at the sample site. This effective production rate can be obtained by calculating an effective R_C for the sample site, which is calculated from the average M/M_0 over the exposure period. Although this approach is less rigorous than the one described above, it can be used to gain an initial estimate of the temporal geomagnetic effect.

Masarik et al. [29] have suggested that geomagnetic corrections calculated by [38] for equatorial stromatolite samples with ages of 8–12 kyr may be too large. According to [38], the correction was approximately +20%, whereas [29] computed a correction of −1%. Our calculations based on the scaling model given here and the Sint-200 record [36] also give a correction that is smaller and in the opposite direction (∼−5%). Because the production rates used by [38] were based mostly on calibration sites at high and mid-latitudes, the production rates at the calibration sites should be mostly independent of dipole intensity. However, near the equator, neutron fluxes were generally greater over the past 8–12 kyr, meaning that production rates were higher and that uncorrected ages would to be too old.

7. Comparison and validation of scaling models

In order to compare scaling models given by [2,4] with the ones derived here, it is necessary to express these models according to common elevation and geomagnetic parameters. Because the models given here and by [4] are already ordered according to atmospheric depth [g cm^{-2}], we expressed Lal's [2] scaling model in terms of atmospheric depth. The US standard atmosphere, 1976, which [2] used to convert his original scaling model [1] from pressure units to elevation units, was used to reverse that transformation. We converted R_C in our models and geomagnetic inclination in Dunai's model [4] to geomagnetic latitude in a centered dipole field having the 1945 dipole intensity, $M_0 = 8.084 \times 10^{22}$ A m^2 [50].

Different latitude effects are given by our sea-level NM-64 curve, Lal's sea-level curve and Dunai's sea-level curve (both derived from [9]) (Fig. 9) because latitude survey data were ordered according to different geomagnetic cutoff parameters by the respective authors [2,4]. Effective vertical cutoff rigidity, used in this work, is the only one that gives a unique relationship for latitude survey data, regardless of the survey route. The shapes of both Lal's and Dunai's latitude curves depend on the longitudes as well as the latitudes covered by the surveys they used [2,4]. Conceivably, the discrepancies in Fig. 9 could have been larger, given the non-unique relations that geomagnetic latitude and geomagnetic inclination have with primary cosmic-ray intensity.

Altitude effects given here are also different

[1] http://www.elsevier.nl/locate/epsl/

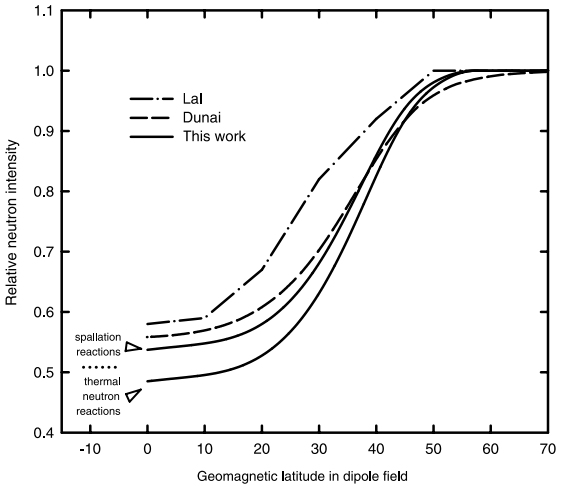

Fig. 9. A comparison of sea-level latitude curves given in this work with ones reported by Lal [2] and Dunai [4]. Geomagnetic latitude corresponds to an axially symmetric centered-dipole representation of the 1945 field ($M_0 = 8.084 \times 10^{22}$ A m^2 [50]).

from those given by [2,4]. Dunai's attenuation lengths are closer to attenuation lengths we give for spallation reactions, whereas Lal's are closer to our thermal neutron attenuation lengths [2,4]. This latter result is expected, since both Lal's model and our model for thermal neutron reactions incorporate data from shielded and unshielded proportional counters, which consistently give higher attenuation lengths than other instruments [2].

Recent measurements of cosmogenic nuclide production in artificial targets [54] afford the opportunity to validate our attenuation length model for spallation reactions at a single R_C and over a small range of atmospheric depths. Three water targets were exposed at 960 g cm^{-2} (620 m), 644 g cm^{-2} (3810 m) and 570 g cm^{-2} (4745 m) on Mount Blanc, France from February, 1993 to May, 1994 ($R_C = 4.82$ GV, geomagnetic latitude = 40.5°, $I = 61.7°$ for epoch 1995) [54]. The effective attenuation length of 130 ± 4 g cm^{-2} measured for ^{10}Be production in oxygen compares well with both the effective attenuation length given in this work for spallation reactions and the attenuation length given by [4] for nuclear reactions (both are 131 g cm^{-2}). A value of 148 g cm^{-2} is obtained for this location from Lal's polynomial for nuclear disintegrations [2]. The neutron monitor data on which our spallation scaling model is based are particularly well-suited to scaling ^{10}Be production because neutron monitors are sensitive to the same portion of the nucleon spectrum that produces the ^{16}O(n,x)^{10}Be reaction (Table 10). Future work with artificial or geological targets should focus on low-latitude, high-altitude locations because this is where discrepancies between scaling models are greatest (Fig. 10).

8. Uncertainty in scaling models

The uncertainty in applying neutron monitor data to scaling factors is difficult to assess [6,7]. Others [3,4] have based their uncertainty estimates on the scatter of data around their regressions. In our model, the 1σ uncertainty is negligible in our weighted fit to the 110 neutron monitor attenuation lengths derived from [11–13]. Before differentiating (Eq. 4) and correcting for muons (Eq. 5) the average 1σ uncertainty in attenuation lengths from our regression is 1%, whereas a weighted average gives 0.1%.

Propagating the uncertainties from the weighted regression through Eqs. 4 and 5 yields a final average 1σ uncertainty of 0.5% in the corrected neutron monitor attenuation lengths ($\Lambda_{NM,N}$) from Eq. 8. This uncertainty assumes that the uncertainties on the relative contributions of muons and nucleons (Table 1) are uncorrelated, and that attenuation lengths for muons

Table 10
Median energies for cosmogenic nuclide production by nucleons [7] and for the neutron monitor response to neutrons [57], both at high latitude and sea level

		E_{med} (MeV)
Reaction	K(n,x)^{36}Cl	13
	Ca(n,x)^{36}Cl	55
	Si(n,x)^{26}Al	70
	O(n,x)^{14}C	105
	O(n,x)^{10}Be	140
Neutron monitor	NM-64	130
	IGY	160

1σ uncertainties are approximately 25%.

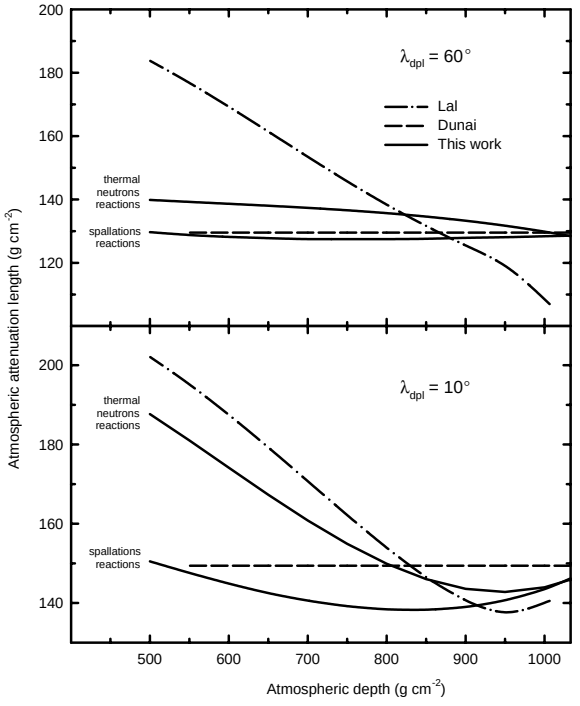

Fig. 10. A comparison of attenuation lengths derived in this work with attenuation lengths calculated from Lal's [2] polynomial for neutron fluxes and attenuation lengths given by Dunai [4]. Geomagnetic latitude is calculated from an axially symmetric centered-dipole field with a dipole moment (M_0) of 8.084×10^{22} A m^2 (1945 value [50]).

(Eqs. 6 and 7) are correct to within an assumed 1σ uncertainty of 20%. The low uncertainty in $\Lambda_{NM,N}$ (Eq. 8) shows only that our regression is an excellent fit to Carmichael's [11–13] data, and that the correction for muons does not substantially increase the uncertainty of our model.

For calculating uncertainties on scaled production rates, an uncertainty of 0.5% in Λ_{sp} is unrealistically low, since it does not account for uncertainties related to biases in energy sensitivity and solar activity. At high latitudes, Λ_{sp} varies by about ~4% over the 11-yr solar cycle (Eq. 13), and instrumental biases in energy sensitivity are small (Fig. 10). At low latitudes, Λ_{sp} is unaffected by solar activity, but uncertainties in the energy bias of Λ_{sp} become important. An average 1σ uncertainty of +5/−2% in Λ_{sp} over all latitudes is therefore recommended as a more realistic estimate for scaling production rates. Uncertainty is lower on the negative side because the neutron monitor is sensitive to higher energies than are most of the important spallation reactions (Table 10), meaning that $\Lambda_{NM,N}$ should give a lower limit for Λ_{sp}. The attenuation length for thermal neutron reactions (Λ_{th}) is not as well-constrained, and a realistic uncertainty is ±6%. Continued efforts are needed to obtain more rigorous and meaningful estimates of uncertainty in scaling models.

9. Conclusions

Our analysis of published cosmic-ray data suggests that separate scaling models should be used for thermal neutron absorption reactions and for spallation reactions. We found that neutron monitors give throughout a wide range of atmospheric depths lower attenuation lengths than do proportional counters. A recent latitude survey shows that neutron monitors also yield a less pronounced latitude effect than do proportional counters. Given that proportional counters measure neutrons at a lower range of energies (mostly neutrons of $E<10$ MeV) than neutron monitors (mostly nucleons of $E>50$ MeV), these findings are consistent with a nucleon energy spectrum that shifts towards lower energies with increasing depth in the atmosphere. If, to the contrary, the shape of the nucleon energy spectrum is invariant in the troposphere, as suggested by recent model calculations [29], then systematic discrepancies between attenuation lengths measured with neutron monitors and those measured in the fast to thermal neutron range must be explained in some other way. Without the assumption of a softening energy spectrum, there is currently no basis to accept one type of neutron measurement over the other.

A rigorous correction for temporal variations in the geomagnetic field can be applied to production rates directly from the scaling models given here. The accuracy of this correction depends mainly on the robustness of altitude–latitude scaling models and on the reliability of the geomagnetic record. The main assumption of our temporal–geomagnetic correction is that at any given

atmospheric depth, cosmic-ray intensity varies uniquely as a function of R_C. For paleomagnetic fields having poorly constrained configurations, as is usually the case in cosmogenic dating, it may be necessary to assume a geocentric axially symmetric dipole field in order to calculate R_C, although this assumption is not intrinsic to our model.

Others working on the scaling aspect of cosmogenic nuclide systematics [4,54–56] seemed to have reached at least one common conclusion with us: that additional theoretical and experimental cosmic-ray research is needed to improve the accuracy and robustness of surface exposure dating, and to open new applications of cosmogenic nuclides.

Acknowledgements

We thank D. Lal and J. Masarik for their helpful comments on the manuscript. We also acknowledge the invaluable assistance provided by V. Radhakrishnan and his staff at Raman Research Insitute for our neutron measurements in India. This material is based upon work supported by the National Science Foundation under Grants EAR-0001191, EAR-0126209 and ATM-0081403 and by Packard Fellowship in Science and Engineering 95-1832.*[RV]*

References

[1] D. Lal, Investigation of nuclear interactions produced by cosmic rays, Ph.D., University of Bombay, 1958.
[2] D. Lal, Cosmic ray labeling of erosion surfaces: in situ nuclide production rates and erosion models, Earth Planet. Sci. Lett. 104 (1991) 424–439.
[3] N. Lifton, A robust scaling model for in situ cosmogenic nuclide production rates, in: Geological Society of America Annual Meeting, abstracts with programs, Reno, NV, 2000, p. A400.
[4] T.J. Dunai, Scaling factors for production rates of in situ produced cosmogenic nuclides: a critical reevaluation, Earth Planet. Sci. Lett. 176 (2000) 157–169.
[5] J.O. Stone, Air pressure and cosmogenic isotope production, J. Geophys. Res. B 105 (2000) 23753–23759.
[6] D. Desilets, M. Zreda, On scaling cosmogenic nuclide production rates for altitude and latitude using cosmic-ray measurements, Earth Planet. Sci. Lett. 193 (2001) 213–225.
[7] D.M. Desilets, The global distribution of secondary cosmic-ray intensity and applications to cosmogenic dating, M.S., University of Arizona, 2001.
[8] D. Desilets, M. Zreda, N.A. Lifton, Comment on 'Scaling factors for production rates of in situ produced cosmogenic nuclides: a critical reevaluation', Earth Planet. Sci. Lett. 188 (2001) 283–287.
[9] D.C. Rose, K.B. Fenton, J. Katzman, J.A. Simpson, Latitude effects of the cosmic ray nucleon and meson components at sea level from the Arctic to the Antarctic, Can. J. Phys. 34 (1956) 968–984.
[10] J.F. Ziegler, Terrestrial cosmic ray intensities, IBM J. Res. Dev. 40 (1996) 19–39.
[11] H. Carmichael, M. Bercovitch, J.F. Steljes, M. Magidin, I. Cosmic-ray latitude survey in North America in summer, 1965, Can. J. Phys. 47 (1969) 2037–2050.
[12] H. Carmichael, M. Bercovitch, II. Cosmic-ray latitude survey in Canada in December, 1965, Can. J. Phys. 47 (1969) 2051–2055.
[13] H. Carmichael, M.A. Shea, R.W. Peterson, III. Cosmic-ray latitude survey in Western USA and Hawaii in summer, 1966, Can. J. Phys. 47 (1969) 2057–2065.
[14] H. Carmichael, M.A. Shea, D.F. Smart, J.R. McCall, IV. Geographically smoothed geomagnetic cutoffs, Can. J. Phys. 47 (1969) 2067–2072.
[15] H. Carmichael, M. Bercovitch, V. Analysis of IQSY cosmic-ray survey measurements, Can. J. Phys. 47 (1969) 2073–2093.
[16] G. Villoresi, L.I. Dorman, N. Iucci, N.G. Ptitsyna, Cosmic ray survey to Antarctica and coupling functions for neutron component near solar minimum (1996-1997) 1. Methodology and data quality assurance, J. Geophys. Res. 105 (2000) 21025–21034.
[17] B.C. Raubenheimer, P.H. Stoker, Attenuation coefficients of various cosmic ray components in the lower atmosphere, in: Proceedings of the 12th International Conference on Cosmic Rays, 1971, pp. 893–896.
[18] F. Bachelet, N. Iucci, G. Villoresi, N. Zangrilli, The cosmic-ray spectral modulation above 2 GV. IV. The influence on the attenuation coefficient of the nucleonic component, Il Nuovo Cimento 11B (1972) 1–12.
[19] N. Iucci, G. Villoresi, L.I. Dorman, M. Parisi, Cosmic ray survey to Antarctica and coupling functions for neutron component near solar minimum (1996-1997) 1. Determination of meteorological effects, J. Geophys. Res. 105 (2000) 21035–21045.
[20] L.I. Dorman, G. Villoresi, N. Iucci, M. Parisi, M.I. Tyasto, O.A. Danilova, N.G. Ptitsyna, Cosmic ray survey to Antarctica and coupling functions for neutron component near solar minimum (1996–1997) 3. Geomagnetic effects and coupling functions, J. Geophys. Res. 105 (2000) 21047–21056.
[21] H. Carmichael, R.W. Peterson, Dependence of the neutron monitor attenuation coefficient on atmospheric depth and on geomagnetic cutoff in 1966 and in 1970, in: Proceedings of the 12th International Cosmic Ray Conference, 1971, pp. 887–892.
[22] C.J. Hatton, H. Carmichael, Experimental investigation

of the NM-64 neutron monitor, Can. J. Phys. 42 (1964) 2443–2472.
[23] F. Ashton, The range-energy relationship for high-energy μ-mesons, Proc. Phys. Soc. 77 (1961) 587–592.
[24] B. Rossi, M. Sands, R.F. Sard, Measurements of slow meson intensity at several altitudes, Phys. Rev. 72 (1947) 120–125.
[25] M. Sands, Low energy mesons in the atmosphere, Phys. Rev. 77 (1950) 180–193.
[26] M. Conversi, Experiments on cosmic-ray mesons and protons at several altitudes and latitudes, Phys. Rev. 79 (1950) 749–767.
[27] O.C. Allkofer, R.D. Andresen, K. Clausen, W.D. Dau, Sea-level muon spectrum at two different latitudes, J. Geophys. Res. 77 (1972) 4251–4253.
[28] T.J. Dunai, Inluence of secular variation of the geomagnetic field on production rates of in situ produced cosmogenic nuclides, Earth Planet. Sci. Lett. 193 (2001) 197–212.
[29] J. Masarik, M. Frank, J.M. Schäfer, W. Rainer, Correction of in situ cosmogenic nuclide production rates for geomagnetic field intensity variations during the past 800,000 years, Geochim. Cosmochim. Acta 65 (2001) 2995–3003.
[30] J.A. Simpson, Neutrons produced in the atmosphere by the cosmic radiations, Phys. Rev. 83 (1951) 1175–1188.
[31] R.K. Soberman, High-altitude cosmic-ray intensity variations, Phys. Rev. 102 (1956) 1399–1409.
[32] M. Merker, E.S. Light, H.J. Verschell, R.B. Mendell, S.A. Korff, Time dependent worldwide distribution of atmospheric neutrons and their products. 1. Fast neutron obervations, J. Geophys. Res. 78 (1973) 2727–2740.
[33] C.F.W. Mischke, Intensiteisvaiasies van neutrone vanaf kosmiese strale, M.S., University of Potchefstroom, 1972.
[34] M.S. Potgeiter, B.C. Raubenheimer, P.H. Stoker, A.J. van der Walt, Modulation of cosmic rays during solar minimum. Part 2. Cosmic ray latitude distribution at sea level during 1976, S. Afr. J. Phys. 3 (1980) 77–89.
[35] B.C. Raubenheimer, P.H. Stoker, Various aspects of the attenuation coefficient of a neutron monitor, J. Geophys. Res. 79 (1974) 5069–5076.
[36] Y. Guyodo, J.P. Valet, Relative variations in geomagnetic intensity from sedimentary records: the past 200,000 years, Earth Planet. Sci. Lett. 143 (1996) 23–26.
[37] J.M. Licciardi, M.D. Kurz, P.U. Clark, E.J. Brook, Calibration of cosmogenic ^{3}He production rates from Holocene lava flows in Oregon, USA, and effects of the Earth's magnetic field, Earth Planet. Sci. Lett. 172 (1999) 261–271.
[38] T.M. Shanahan, M. Zreda, Chronology of Quaternary glaciations in East Africa, Earth Planet. Sci. Lett. 177 (2000) 23–42.
[39] M.W. McElhinny, W.E. Senanayake, Variations in the geomagnetic dipole I: the past 50,000 years, J. Geomagn. Geoelectr. 34 (1982) 39–51.
[40] M. Ohno, Y. Hamano, Geomagnetic poles over the past 10,000 years, Geophys. Res. Lett. 19 (1992) 1715–1718.
[41] M. Ohno, Y. Hamano, Global analysis of the geomagnetic-field time variation of the dipole moment and the geomagnetic pole in the Holocene, J. Geomagn. Geoelectr. 45 (1993) 1455–1466.
[42] Y. Guyodo, J.P. Valet, Global changes in intensity of the Earth's magnetic field during the past 800 kyr, Nature 399 (1999) 249–252.
[43] P.R. Bierman, E.M. Clapp, Estimating geologic age from cosmogenic nuclides: an update, Science 271 (1996) 1606.
[44] F.M. Phillips, M.G. Zreda, M.R. Flinsch, D. Elmore, P. Sharma, A reevaluation of cosmogenic ^{36}Cl production rates in terrestrial rocks, Geophys. Res. Lett. 23 (1996) 949–952.
[45] W. Elsasser, E.P. Ney, J.R. Winckler, Cosmic-ray intensity and geomagnetism, Nature 178 (1956) 1226–1227.
[46] D. Lal, B. Peters, Cosmic ray produced radioactivity on Earth, in: K. Sitte, Ed., Encyclopedia of Physics: Cosmic Rays II, Encyclopedia of Physics, vol. 46/2, Springer, Berlin, 1967, pp. 551–612.
[47] D. Lal, In situ-produced cosmogenic isotopes in terrestrial rocks, Annu. Rev. Earth Planet. Sci. 16 (1988) 355–388.
[48] P. Rothwell, Cosmic rays in the Earth's magnetic field, Philos. Mag. 3 (1958) 961–970.
[49] M.A. Shea, D.F. Smart, K.G. McCracken, A study of vertical cutoff rigidities using sixth degree simulations of the geomagnetic field, J. Geophys. Res. 70 (1965) 4117–4130.
[50] A.C. Fraser-Smith, Centered and eccentric geomagnetic dipoles and their poles, 1600-1985, Rev. Geophys. 25 (1987) 1–16.
[51] M.A. Shea, D.F. Smart, A world grid of calculated cosmic ray vertical cutoff rigidities for 1980.0, in: Proceedings of the 18th International Cosmic Ray Conference MG 10-3, Bangalore, India, 1983, pp. 415–418.
[52] M.G. Zreda, F.M. Phillips, Surface exposure dating by cosmogenic chlorine-36 accumulation, in: C. Beck, Ed., Dating in Exposed and Surface Contexts, University of New Mexico Press, 1994, pp. 161–183.
[53] F.M. Phillips, W.D. Stone, J.T. Fabryka-Martin, An improved approach to calculating low-energy cosmic-ray neutron fluxes near the land/atmosphere interface, Chem. Geol. 175 (2001) 689–701.
[54] E.T. Brown, T.W. Trull, P. Jean-Baptiste, G. Raisbeck, D. Bourlès, F. Yiou, B. Marty, Determination of cosmogenic production rates of ^{10}Be, ^{3}He and ^{3}H in water, Nucl. Instrum. Methods B 172 (2000) 873–883.
[55] D. Lal, Cosmogenic nuclide production rate systematics in terrestrial materials: Present knowledge, needs and future actions for improvement, Nucl. Instrum. Methods B 172 (2000) 772–781.
[56] I.J. Graham, B.J. Barry, R.G. Ditchburn, N.E. Whitehead, Validation of cosmogenic nuclide production rate scaling factors through direct measurement, Nucl. Instrum. Methods B 172 (2000) 802–805.
[57] C.J. Hatton, The neutron monitor, in: J.G. Wilson and S.A. Wouthuysen, Eds., Progress in Elementary Particle

and Cosmic Ray Physics, vol. 10, North-Holland, Amsterdam, 1971, pp. 1–100.

[58] O.C. Allkofer, R.D. Andresen, E. Bagge, W.D. Dau, H. Funk, Der Einfluss des Erdmagnetfeldes auf die kosmische Strahlung, 1, Untersuchungen der Nukleonenkomponente der kosmische Strahlung waehrend der atlantischen Expedition IQSY 1965 auf dem Forschungsschif 'Meteor', in: 'Meteor' Forschungsergebnisse, Reihe B, Heft 3, Gebrüder Borntraeger, Berlin, 1969.

[59] T.M. Aleksanyan, I.V. Dorman, L.I. Dorman, V.K. Babayan, A.V. Belov, Y.L. Blokh, N.S. Kaminer, V.K. Korotkov, I.Y. Libin, A.A. Manshilina, Y.E. Mashkov, I.V. Mymrina, S.I. Rogovaya, A.M. Sitnov, K.F. Yudakhin, V. Yanke, Geomagnetic effects in cosmic rays and spectrum of the increase before magnetic storms, Izv. Akad. Nauk SSSR Ser. Fiz. 46 (1982) 1689–1691.

[60] P.H. Stoker, A.J. van der Walt, M.S. Potgieter, Modulation of cosmic rays during solar minimum, 1, Cosmic ray intensity survey at sea-level during 1976: Experimental details, S. Afr. J. Phys. 3 (1980) 73–76.

[61] H. Moraal, M.S. Potgieter, P.H. Stoker, Neutron monitor latitude survey of cosmic ray intensity during the 1986/1987 solar minimum, J. Geophys. Res. 94 (1989) 1459–1464.

[62] M.A. Shea, D.F. Smart, J.R. McCall, A five degree by fifteen degree world grid of trajectory-determined vertical cutoff rigidities, Can. J. Phys. 46 (1968) S1098–S1101.